Volume 15
Number 24
21 December 2025
Pages 7253–7560

Catalysis Science & Technology

rsc.li/catalysis

ISSN 2044-4761

ROYAL SOCIETY OF CHEMISTRY

PAPER

Atsuhiro Tanaka, Hiroshi Kominami *et al.*
Preparation of RhO_x/TiO_2 with Pt cocatalyst effective for photocatalytic alcohol dehydrogenation under irradiation of visible light

Catalysis Science & Technology

ROYAL SOCIETY OF CHEMISTRY

PAPER

View Article Online
View Journal | View Issue

Check for updates

Cite this: *Catal. Sci. Technol.*, 2025, 15, 7333

Preparation of RhO_x/TiO_2 with Pt cocatalyst effective for photocatalytic alcohol dehydrogenation under irradiation of visible light

Atsuhiro Tanaka, * Masaaki Fukuda, Takumi Nagai, Hiroyuki Asakura and Hiroshi Kominami *

Photocatalytic alcohol dehydrogenation is a promising technique for the simultaneous production of hydrogen (H_2) and carbonyl compounds. In this study, titanium(IV) oxide (TiO_2) photocatalysts co-loaded with rhodium oxide (RhO_x) and platinum (Pt) particles were successfully prepared *via* a multi-step process involving the equilibrium adsorption of Rh ions, post-calcination, and Pt colloid impregnation. In the resulting system, RhO_x acts as a visible-light sensitizer, while Pt serves as the hydrogen evolution co-catalyst. A series of RhO_x/TiO_2–Pt samples were synthesized by systematically varying the calcination temperature of the RhO_x/TiO_2 precursor prior to Pt loading. These materials were then evaluated for photocatalytic alcohol dehydrogenation under visible light irradiation. The effects of calcination temperature on the electronic states and light absorption characteristics of the Rh species were investigated, along with their influence on photocatalytic activity. The RhO_x/TiO_2–Pt photocatalysts exhibited efficient dehydrogenation of various alcohols. In particular, benzyl alcohol was selectively converted to benzaldehyde and H_2 in a stoichiometric ratio, with no over-oxidation observed. This work demonstrates a novel strategy for coupling oxidative organic synthesis with hydrogen production under visible light, offering new insights into photocatalyst design for sustainable energy and chemical synthesis.

Received 7th August 2025,
Accepted 22nd October 2025

DOI: 10.1039/d5cy00963d

rsc.li/catalysis

Open Access Article. Published on 22 October 2025. Downloaded on 4/23/2026 1:04:59 PM.
This article is licensed under a Creative Commons Attribution-NonCommercial 3.0 Unported Licence.

1. Introduction

Extensive research has been devoted to the development of TiO_2-based photocatalysts that respond to visible light. This sustained interest is driven by several key factors, among which the following three stand out:

1. TiO_2 exhibits exceptional and unrivaled photocatalytic properties;

2. Titanium is an abundant and safe element, making it attractive from both environmental and resource-availability perspectives;

3. There is a strong demand to harness visible light, in addition to ultraviolet (UV) light, for practical photocatalytic applications.

Therefore, narrowing the band gap of TiO_2 or sensitizing it to visible light is a critical challenge. Various approaches have been explored, such as creating oxygen vacancies, elemental doping (both cationic and anionic), and forming heterostructures.[1] Although these methods have successfully improved visible-light absorption, they sometimes introduce charge recombination centers or exhibit thermal instability. In this context, surface modification has emerged as a simple and effective strategy for enabling wide-bandgap TiO_2 to absorb visible light. A variety of surface modifiers have been explored, including transition metals in different chemical forms, halides,[2] hydroxides,[3] metal ions,[4] and oxides,[5] as well as metal complexes[6] and organic compounds.[7] In these modified TiO_2 systems, the modifying species are not incorporated into the crystal lattice but are instead supported on the surface of the TiO_2 particles. This surface configuration facilitates efficient charge transfer between the modifiers and TiO_2 (Fig. 1). Importantly, the surface-bound

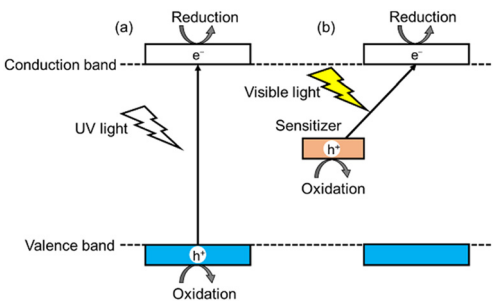

Fig. 1 Proposed energy diagram; (a) band-gap excitation of TiO_2 and (b) charge transfer from a sensitizer to the CB of TiO_2.

Department of Applied Chemistry, Faculty of Science and Engineering, Kindai University, Kowakae, Higashiosaka, Osaka 577-8502, Japan.
E-mail: atsu.tana@apch.kindai.ac.jp, hiro@apch.kindai.ac.jp

Open Access Article. Published on 22 October 2025. Downloaded on 4/23/2026 1:04:59 PM.
This article is licensed under a Creative Commons Attribution-NonCommercial 3.0 Unported Licence.

species serve dual roles as visible light absorption centres and oxidation sites.

When TiO_2-based photocatalysts are employed for degradation or oxidation reactions under aerated conditions, molecular oxygen (O_2) acts as an effective electron scavenger. The conduction band (CB) potential of TiO_2 (~−0.3 V *vs.* NHE) is sufficiently negative to drive the reduction of O_2, allowing these reactions to proceed without the need for further modification. For instance, TiO_2 modified with rhodium (Rh) ions has been shown to degrade volatile organic compounds (VOCs) under visible light irradiation.[8] Moreover, selective oxidation of aromatic alcohols has been achieved using TiO_2 modified with Rh, palladium (Pd), and ruthenium (Ru) ions.[9] The structural evolution of Rh species on TiO_2 and their influence on photocatalytic performance have also been studied in detail. It was found that calcination-induced changes in RhO_x/TiO_2 can significantly affect activity without altering the intrinsic physical properties of TiO_2.[10] Notably, atomically isolated Rh^{3+} species were identified as the most active form, while aggregation of Rh species led to a marked decline in photocatalytic efficiency.

When TiO_2-based photocatalysts (including both unmodified and modified forms) are used for the reduction of a compound under deaerated conditions in the presence of an electron donor, the compound accepts photogenerated electrons either directly or indirectly. In most cases, the incorporation of a co-catalyst is essential to achieve a practical reaction rate and high selectivity for the desired product. A representative example is the hydrogen (H_2) evolution reaction. Given the relatively low overpotential for hydrogen evolution, platinum (Pt) is widely recognized as the most effective co-catalyst. In other systems, the choice of co-catalyst significantly influences selectivity. For instance, in the selective reduction of nitrates to ammonia using an aqueous suspension of a TiO_2 photocatalyst, copper (Cu) co-catalysts demonstrated superior selectivity.[11] Similarly, silver (Ag) co-catalysts exhibited high activity for the deoxygenation of epoxides in alcoholic suspensions of TiO_2 photocatalysts.[12] When a modified TiO_2 photocatalyst is used in conjunction with a co-catalyst, both the visible-light sensitizer (modifier) and the co-catalyst must be introduced onto the TiO_2 surface. To ensure efficient photocatalytic performance, it is critical to prevent interference between these two components. Therefore, specialized preparation methods are required to preserve and optimize the individual functions of the modifier and the co-catalyst.

Many researchers have reported H_2 production from various compounds using TiO_2 photocatalysts under UV irradiation.[13] This approach represents a promising and environmentally friendly technology for generating clean energy from renewable resources. However, UV light accounts for only about 5% of the total solar spectrum, whereas visible light contributes approximately 50%. Consequently, significant research has focused on developing visible-light-responsive photocatalysts for H_2 production.[14]

Photocatalytic alcohol dehydrogenation has emerged as a particularly attractive route for H_2 generation.[15] One advantage is its favourable thermodynamics compared to water splitting. For instance, the standard Gibbs free energy change ($\Delta_r G^0$) for ethanol dehydrogenation ($C_2H_5OH(l) \rightarrow CH_3CHO(l) + H_2(g)$) is 47 kJ mol^{-1}, substantially lower than that for water splitting ($\Delta_r G^0$ = 237 kJ mol^{-1}). Additionally, alcohol dehydrogenation produces a valuable carbonyl compound as an oxidation product without requiring any additives. In contrast, achieving selective oxidation to carbonyl compounds using conventional oxidants such as oxygen or permanganate is often challenging. In this study, we applied RhO_x/TiO_2 photocatalysts for H_2 evolution *via* alcohol dehydrogenation under visible light irradiation. To meet the dual requirements of visible-light absorption and efficient hydrogen evolution, a new preparation method was employed. Specifically, Pt colloids were loaded onto RhO_x/TiO_2 to introduce small Pt co-catalyst particles. As anticipated, the resulting RhO_x/TiO_2–Pt samples exhibited significantly higher reaction rates compared to co-catalyst-free RhO_x/TiO_2 under visible light irradiation. Here, we report the characterization of photocatalysts prepared under various conditions and evaluate their catalytic performance in the dehydrogenation of alcohols under visible light irradiation.

2. Experimental section

2.1 Synthesis of TiO_2

Nanocrystalline TiO_2 powder was synthesized *via* hydrothermal crystallization in organic media (HyCOM) at 300 °C.[16] Titanium(IV) butoxide and toluene were used as the titanium precursor and solvent, respectively. The resulting product was calcined at various temperatures for 1 h in a box furnace. Calcination improved the crystallinity of the HyCOM-TiO_2 samples while maintaining a high specific surface area up to 89 m^2 g^{-1} even after treatment at 500 °C. The TiO_2 sample calcined at 500 °C was used in most of the subsequent experiments as the support material for Rh species. To investigate the effect of TiO_2 properties, the HyCOM-TiO_2 sample was calcined at different temperatures. The corresponding pre-calcination temperature (T_1) is indicated in parentheses following TiO_2; for example, TiO_2(700) refers to the sample calcined at 700 °C.

2.2 Preparation of RhO_x/TiO_2

The TiO_2 sample was modified with Rh^{3+} ions using an equilibrium adsorption method. Pre-calcined TiO_2 powder was added to an aqueous solution of rhodium(III) chloride ($RhCl_3$), in an amount corresponding to 1.0 wt% Rh metal. The mixture was stirred and heated in a water bath at approximately 85 °C. After equilibration, the suspension was filtered, and the resulting filter cake was thoroughly washed with distilled water to remove residual chloride ions. The solid was then dried under vacuum for 1 h to obtain the Rh^{3+}/TiO_2 sample. The complete adsorption of Rh^{3+} onto the TiO_2 surface was confirmed by analyzing the filtrate using

 This journal is © The Royal Society of Chemistry 2025

Open Access Article. Published on 22 October 2025. Downloaded on 4/23/2026 1:04:59 PM. This article is licensed under a Creative Commons Attribution-NonCommercial 3.0 Unported Licence.

inductively coupled plasma atomic emission spectroscopy (ICP-OES, Thermo Fisher Scientific Inc., iCAP7600D), which detected no remaining Rh^{3+} in the solution. To modify the structure of the Rh^{3+} species on the TiO_2 surface, the Rh^{3+}/TiO_2 samples were subjected to post-calcination at various temperatures (T_2) for 1 h. This thermal treatment converted the highly dispersed Rh^{3+} species into RhO_x species on the TiO_2 surface. The resulting photocatalysts are denoted as $RhO_x/TiO_2(T_1–T_2)$, where T_1 and T_2 represent the pre- and post-calcination temperatures, respectively. For example, the sample pre-calcined at 500 °C and post-calcined at 400 °C is referred to as RhO_x/TiO_2(500–400).

2.3 Platinization of RhO_x/TiO_2

Colloidal Pt nanoparticles were prepared according to the method reported by Frens.[17] An aqueous solution of hexachloroplatinic(IV) acid (H_2PtCl_6, 0.0402 g cm^{-3}, 750 cm^3) was mixed with 100 cm^3 of an aqueous sodium citrate solution (39 mmol dm^{-3}). The mixture was heated to boiling and maintained at reflux for 1 h. As the reaction proceeded, the solution color changed from yellow to deep gray, indicating the formation of Pt nanoparticles. Boiling was continued for an additional 30 min to ensure complete reduction. After cooling to room temperature, 50 cm^3 of Amberlite MB-1 ion exchange resin (ORGANO) was added to the solution to remove excess sodium citrate. After 1 h of treatment, the resin was removed by filtration using a glass filter. Pt loading onto the RhO_x/TiO_2 samples was carried out *via* the colloid salting-out (CS) method.[18] A typical preparation of RhO_x/TiO_2 loaded with 0.5 wt% Pt is described as follows: RhO_x/TiO_2 powder (150 mg) was suspended in 20 cm^3 (0.754 mg) of the prepared colloidal Pt solution and stirred at room temperature for 30 min in a centrifuge tube. Then, approximately 1 g of ammonium chloride was added to the mixture, which was stirred for an additional 30 min to induce deposition of the Pt nanoparticles onto the TiO_2 surface. The resulting solid was collected, washed thoroughly with distilled water to remove residual salts, and air-dried. The final platinized photocatalysts are denoted as $RhO_x/TiO_2(T_1–T_2)$–Pt(Y), where Y represents the Pt loading (*e.g.*, 0.5 wt%).

2.4 Characterization

Diffuse reflectance spectra of the RhO_x/TiO_2 samples were recorded using a UV-visible spectrophotometer (UV-2600, Shimadzu, Kyoto) equipped with a diffuse reflectance accessory (ISR-2600Plus, Shimadzu). The morphology of the samples was examined by transmission electron microscopy (TEM) using a JEOL JEM-2100F microscope operated at 200 kV at the Joint Research Center (JRC) of Kindai University. Rhodium K-edge X-ray absorption fine structure (XAFS) measurements were conducted in transmission mode at beamline BL01B1 of the SPring-8 synchrotron radiation facility (Hyogo, Japan). Standard data processing procedures, including background subtraction and normalization, were performed using Athena[19] (version 0.9.26). Powder X-ray diffraction of TiO_2 was recorded on a MiniFlex (Rigaku, Tokyo, Japan) in the JRC at Kindai University using CuKα radiation with a monochromator.

2.5 Hydrogen formation by dehydrogenation of 2-propanol

In this study, the dehydrogenation of 2-propanol, *i.e.*, producing hydrogen (H_2) and acetone, was selected as a model reaction under visible light irradiation, as shown in eqn (1):

$$(CH_3)_2CHOH \rightarrow (CH_3)_2CO + H_2. \quad (1)$$

Dried photocatalyst powder (50 mg) was suspended in 5 cm^3 of 2-propanol, degassed by bubbling with Ar, and sealed with a rubber septum. The suspension was then irradiated under visible light using a 500 W xenon (Xe) lamp (Eagle Engineering, Tokyo) equipped with a Y-43 cutoff filter (HOYA Corporation, Tokyo), while magnetically stirred in a water bath maintained at 25 °C. The amount of H_2 generated in the gas phase was measured using a Shimadzu GC-8A gas chromatograph equipped with an MS-5A column. Acetone produced in the liquid phase was quantified using a Shimadzu GC-2025 gas chromatograph fitted with a DB-WAX column, with toluene used as an internal standard.

3. Results and discussion

3.1 Characterization of samples

Fig. 2 shows the UV-vis absorption spectra of TiO_2, TiO_2–Pt(0.5), RhO_x/TiO_2(500–400), and RhO_x/TiO_2(500–400)–Pt(0.5) samples. The unmodified TiO_2 exhibited absorption only below 400 nm, consistent with its intrinsic bandgap excitation. Upon deposition of Pt particles, TiO_2–Pt(0.5) showed a baseline increase in photoabsorption, typically accompanied by a visible color change from white to gray. The RhO_x/TiO_2(500–400) sample displayed additional absorption in the 400–600 nm range, attributed to the presence of Rh_2O_3 nanoparticles.[10] In the RhO_x/TiO_2(500–400)–Pt(0.5) sample, both RhO_x and Pt contributed to enhanced photoabsorption, resulting in a broader and more

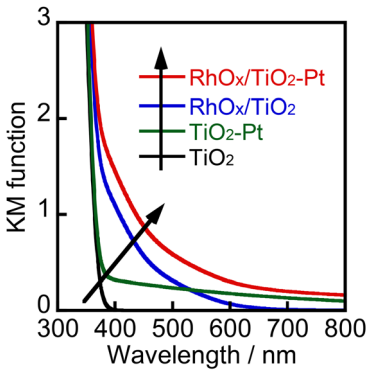

Fig. 2 UV-vis diffuse reflection spectra of various samples.

Open Access Article. Published on 22 October 2025. Downloaded on 4/23/2026 1:04:59 PM.
This article is licensed under a Creative Commons Attribution-NonCommercial 3.0 Unported Licence.

intense absorption profile. Fig. S1 (SI) presents a TEM image and particle size distribution of the colloidal Pt particles, indicating an average particle diameter of 2.9 nm with a relatively narrow size distribution (standard deviation: 1.1 nm). Fig. S2 (SI) shows a TEM image of the RhO_x/TiO_2(500–400)–Pt(0.5) sample prepared *via* the CS method using a Pt colloidal solution. Pt particles were clearly observed on the TiO_2 surface, with an average diameter of 2.8 nm, closely matching the original size of the colloidal Pt particles prior to loading (Fig. S1, SI).

3.2 Formation of H_2 by dehydrogenation of 2-propanol

The photocatalytic activity of TiO_2, TiO_2–Pt(0.5), RhO_x/TiO_2(500–400), and RhO_x/TiO_2(500–400)–Pt(0.5) was evaluated for H_2 production *via* the dehydrogenation of 2-propanol under visible light irradiation. The experiments were conducted at 25 °C using an Xe lamp equipped with a Y-43 cutoff filter. The spectrum of the light from the Xe lamp with the Y-43 cut-off filter used for this reaction is shown in Fig. S3 (SI). The resulting H_2 generation rates for the various photocatalysts are presented in Fig. 3. No H_2 evolution was observed for TiO_2 or TiO_2–Pt(0.5). This result is expected, as the Y-43 cutoff filter blocks UV light, preventing bandgap excitation of TiO_2, and the thermal catalytic activity of Pt is negligible under these conditions. In contrast, the RhO_x/TiO_2(500–400) sample generated H_2 at a rate of 1.3 μmol h^{-1}, demonstrating visible-light-driven photocatalytic activity due to the presence of Rh species. Notably, the RhO_x/TiO_2(500–400)–Pt(0.5) sample showed a significantly enhanced H_2 production rate of 2.8 μmol h^{-1}, indicating that Pt particles effectively function as co-catalysts for H_2 evolution in this system. To confirm that this reaction proceeds *via* photocatalysis and not thermocatalysis, the RhO_x/TiO_2(500–400)–Pt(0.5) sample was also tested under dark conditions at 25 °C. As shown in Fig. 3, no H_2 was detected, confirming that thermal dehydrogenation of 2-propanol is negligible at this temperature. To further evaluate the roles of Rh species and Pt particles, separate samples of RhO_x/TiO_2(500–400) and TiO_2(500)–Pt(0.5) (25 mg each) were physically mixed and irradiated under the same conditions. The resulting H_2 evolution rate was 0.51 μmol h^{-1}, which is approximately half that of RhO_x/TiO_2(500–400) alone (1.3 μmol h^{-1}). This finding highlights the importance of co-loading both Rh species and Pt particles onto the same TiO_2 support to achieve synergistic enhancement and maximize photocatalytic H_2 production from 2-propanol dehydrogenation.

3.3 Time courses of H_2 and acetone produced by 2-propanol dehydrogenation

Fig. 4 shows the time-dependent production of H_2 and acetone during the photocatalytic dehydrogenation of 2-propanol over the RhO_x/TiO_2(500–400)–Pt(0.5) sample. The reaction was carried out under deaerated conditions and visible light irradiation using an Xe lamp equipped with a Y-43 cutoff filter. Immediately upon light irradiation, both H_2 and acetone were generated from the suspension. As irradiation time increased, the amounts of H_2 and acetone increased linearly. The formation rates were determined to be 2.8 μmol h^{-1} for H_2 and 2.7 μmol h^{-1} for acetone. The close agreement between the production rates of H_2 and acetone confirms that the dehydrogenation of 2-propanol proceeded stoichiometrically, as shown in eqn (1). To assess the photocatalyst's stability, the RhO_x/TiO_2–Pt sample was reused in repeated cycles, as shown in Fig. S4 (SI). After each cycle, the reaction mixture was purged with Ar and irradiated again under the same conditions. H_2 evolution resumed without any noticeable decline in activity, even after prolonged irradiation, demonstrating the excellent durability of the catalyst. The total amount of H_2 produced reached approximately 47 μmol, which exceeds the stoichiometric

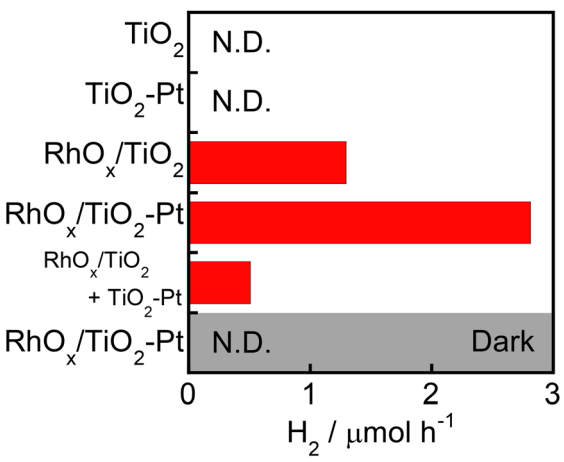

Fig. 3 Rate of H2 formation from 2-propanol suspension of various photocatalysts.

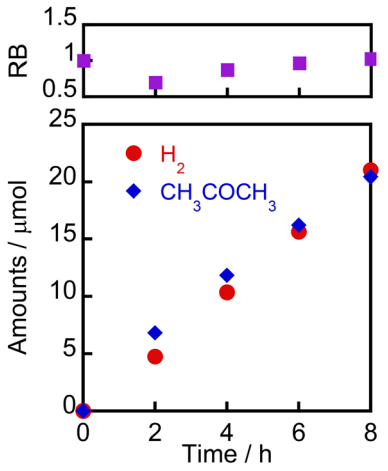

Fig. 4 Time courses of amounts of H_2 and acetone in 2-propanol suspensions of RhO_x/TiO_2(500–400)–Pt under irradiation of light from Xe lamp with cut filter Y-43.

This journal is © The Royal Society of Chemistry 2025

Open Access Article. Published on 22 October 2025. Downloaded on 4/23/2026 1:04:59 PM. This article is licensed under a Creative Commons Attribution-NonCommercial 3.0 Unported Licence.

amount of Rh present in the catalyst (4.9 μmol, corresponding to 1.0 wt%). This clearly indicates that H_2 evolution was not due to a chemical reaction between Rh species and 2-propanol, but rather was the result of a true (photo)catalytic process. The results of XPS and UV-vis for the RhO_x/TiO_2–Pt sample before and after the photocatalytic H_2 formation reaction under visible-light irradiation are shown in Fig. S5 and S6 (SI). In both cases, no changes in the spectra caused by the photocatalytic reaction were observed, clearly demonstrating that the catalyst in this study was stably driven.

3.4 Effect of post-calcination temperature (T_2)

The structure of rhodium species was altered by varying the post-calcination temperature (T_2), and its effect on the photocatalytic dehydrogenation of 2-propanol was investigated. Fig. 5a shows the UV-vis diffuse reflectance spectra of $RhO_x/TiO_2(500–T_2)$ samples calcined at different temperatures. All samples exhibited visible-light absorption, with the intensity increasing as the calcination temperature rose. This enhanced photoabsorption was attributed to structural changes in the Rh species immobilized on the TiO_2 surface, rather than modifications in the bulk properties of the TiO_2 support caused by calcination. In the case of $Rh^{3+}/TiO_2(500)$ without post-calcination, previous studies have shown that Rh species exist as surface complexes coordinated to TiO_2 surface hydroxyl groups, hydroxide ions, and water molecules. The positive charge of Rh^{3+} is balanced by these surface groups, including terminal oxygen atoms and hydroxyls on the TiO_2 surface.[10] During post-calcination, coordinated hydroxide ions and water molecules are gradually removed, which is believed to enhance the interaction between Rh species and the TiO_2 surface. This improved interaction likely facilitates more effective charge transfer between the Rh species and TiO_2, leading to stronger visible-light absorption. The formation of Rh_2O_3 nanoparticles due to Rh species aggregation during calcination is also considered a plausible contributor to this absorption enhancement. To investigate changes in the electronic structure of Rh species, XAFS measurements were performed. Fig. 5b presents the Rh K-edge XANES spectra of commercial Rh foil, Rh_2O_3, and both uncalcined and calcined RhO_x/TiO_2 samples. The spectra of Rh^{3+}/TiO_2 and $RhO_x/TiO_2(500–T_2)$ were similar to that of Rh_2O_3, but clearly different from that of Rh foil. The absorption edge energies of both uncalcined and post-calcined samples closely matched that of Rh_2O_3, indicating that the Rh species predominantly remained in the trivalent oxidation state. Fig. 5c shows H_2 production rates from 2-propanol dehydrogenation using platinized $RhO_x/TiO_2(500–T_2)$ samples. In all cases, H_2 was generated, and the yield increased with increasing T_2 up to 400 °C. The sample calcined at 400 °C exhibited the highest activity, producing 8.4 μmol of H_2 after 3 h. This improvement in photocatalytic activity is attributed to the enhanced visible-light absorption associated with structural changes in Rh species. However, at calcination temperatures above 400 °C, H_2 production decreased, likely due to excessive aggregation of Rh species, which reduces the active surface area and impairs charge transfer efficiency.

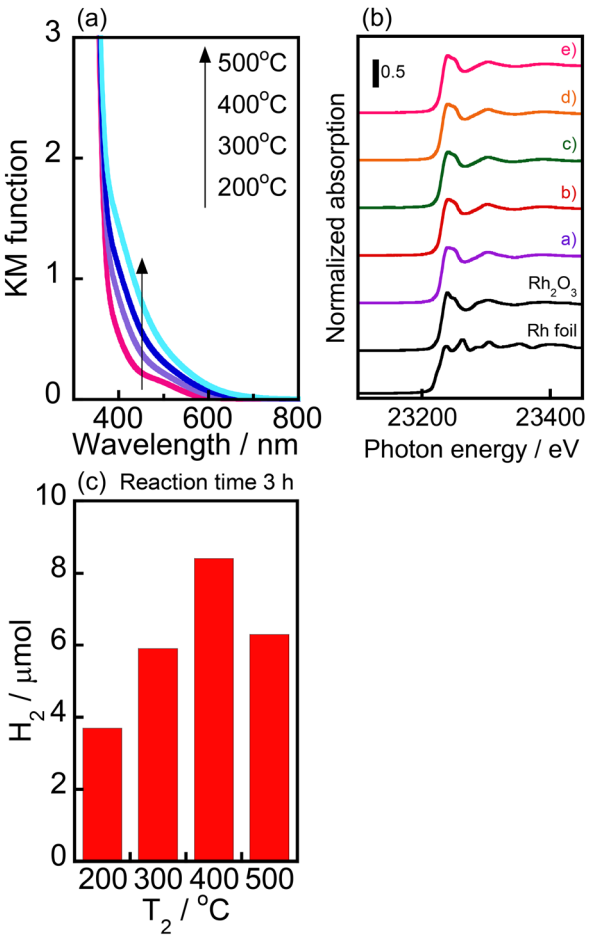

Fig. 5 (a) UV-vis diffuse reflection spectra of $RhO_x/TiO_2(500–T_2)$, (b) Rh K-edge XANES spectra of Rh foil, Rh_2O_3, a) Rh^{3+}/TiO_2, b) $RhO_x/TiO_2(500–200)$, c) $RhO_x/TiO_2(500–300)$, d) $RhO_x/TiO_2(500–400)$ and e) $RhO_x/TiO_2(500–500)$ and (c) amounts of H_2 in 2-propanol suspensions of $RhO_x/TiO_2(500–T_2)$–Pt(0.5) under irradiation of light from Xe lamp with cut filter Y-43 for 3 h.

3.5 Action spectrum

The action spectrum has become increasingly important in the study of visible-light-responsive photocatalysis, as it represents the efficiency of light utilization as a function of wavelength. This metric is critical for identifying both the effective wavelength range and the underlying photoactivation mechanisms in a given photocatalytic system. To evaluate the action spectrum of the current system, 2-propanol dehydrogenation over $RhO_x/TiO_2(500–400)$–Pt(0.5) was conducted at 25 °C under monochromatic visible light irradiation. Light was provided by an Xe lamp equipped with a monochromator (bandwidth ±10 nm). The

Open Access Article. Published on 22 October 2025. Downloaded on 4/23/2026 1:04:59 PM.
This article is licensed under a Creative Commons Attribution-NonCommercial 3.0 Unported Licence.

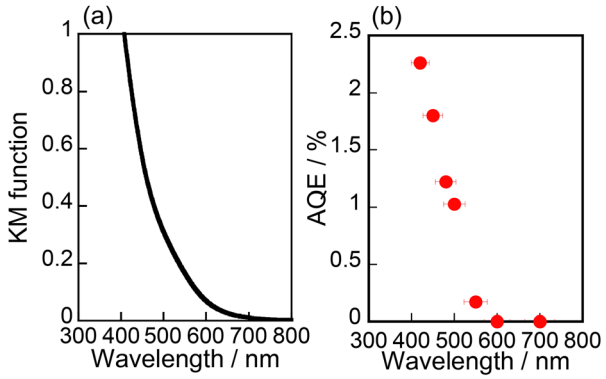

Fig. 6 (a) UV-vis diffuse reflection spectra of RhO_x/TiO_2(500–400), and (b) action spectrum of RhO_x/TiO_2(500–400)–Pt in formation of H_2 from 2-propanol.

apparent quantum efficiency (AQE) at each central wavelength was calculated using eqn (2), which relates the rate of H_2 formation to the photon flux:

$$\mathrm{AQE} = \frac{\text{rate of } H_2 \text{ formation}}{\text{rate of incident photons}} \times 100 \qquad (2)$$

The results are shown in Fig. 6. The AQE values as a function of wavelength for RhO_x/TiO_2–Pt closely matched those for RhO_x/TiO_2, indicating that H_2 evolution was primarily driven by photoabsorption associated with Rh species on the TiO_2 surface. These results confirm that the RhO_x/TiO_2(500–400)–Pt(0.5) photocatalyst is active under visible light irradiation up to 550 nm, consistent with the visible-light absorption properties introduced by the Rh species.

3.6 Effect of physical properties of TiO_2 and the amount of Pt co-catalyst

The effect of pre-calcination temperature (T_1) on the catalytic performance of RhO_x/TiO_2(T_1–400)–Pt(0.5) was investigated. Pre-calcination influences the physical properties and crystal structure of the TiO_2 support. The XRD patterns of TiO_2 samples calcined at different temperatures are shown in Fig. S7 (SI). All the diffraction patterns for the samples calcined in the 400–800 °C range were characteristic of the anatase TiO_2 phase (JCPDS No. 21-1272). Table 1 summarizes the H_2 yields after 3 h of visible light irradiation, along with the specific surface area and crystalline phase of TiO_2 prior to Rh^{3+} modification. All samples showed measurable H_2 production, with activity generally correlating with the specific surface area of the TiO_2, regardless of its crystalline phase. Among the tested samples, RhO_x/TiO_2(500–400)–Pt(0.5), which utilized anatase-type TiO_2, exhibited the highest H_2 yield of 8.4 μmol after 3 h.

To evaluate the influence of Pt loading on the H_2 evolution rate, a series of RhO_x/TiO_2(500–400)–Pt(Y) photocatalysts with varying Pt contents (Y) were prepared. The corresponding H_2 yields under visible light irradiation (after 3 h) are also shown in Table 1 (entries 1 and 5–10). The Pt-free RhO_x/TiO_2(500–400) sample produced only a small amount of H_2 (1.8 μmol), consistent with previous results. A low Pt loading of just 0.2 wt% significantly enhanced H_2 evolution (3.8 μmol), indicating that Pt nanoparticles function efficiently as electron sinks (reduction sites). The H_2 yield continued to increase with Pt loading, reaching a maximum of 8.4 μmol at 0.5 wt% Pt. However, further increases in Pt content ($Y > 0.5$ wt%) resulted in decreased activity. TEM and chemical analysis of the liquid phase confirmed that all Pt particles prepared by the CS method were successfully loaded onto TiO_2 without size variation. Therefore, higher Pt loadings correspond to a greater number of Pt particles, not larger particles. The decline in photocatalytic activity at Pt loadings above 0.5 wt% is attributed to increased light scattering by the excess Pt particles, which reduces the efficiency of light absorption by the active RhO_x/TiO_2 component.

3.7 H_2 production by dehydrogenation of various alcohols

To explore the versatility of the RhO_x/TiO_2–Pt photocatalyst for alcohol dehydrogenation under visible light, a range of alcohols were tested as substrates. As summarized in Table 2, the RhO_x/TiO_2(500–400)–Pt(0.5) photocatalyst was effective in promoting the dehydrogenation of various types of alcohols, including primary aliphatic alcohols (methanol, ethanol,

Table 1 Specific surface area and crystalline phase of TiO_2 before the modification with Rh^{3+} and the amount of H_2 produced from 2-propanol suspensions of RhO_x/TiO_2(T_1–400)–Pt(Y) under irradiation of light from Xe lamp with cut filter Y-43 for 3 h

Entry	Sample	S_{BET}/m^2 g^{-1}	Crystal structure[a]	H_2 yield/μmol
1	RhO_x/TiO_2(500–400)–Pt(0.5)	89	A	8.4
2	RhO_x/TiO_2(600–400)–Pt(0.5)	68	A	7.2
3	RhO_x/TiO_2(700–400)–Pt(0.5)	40	A	5.3
4	RhO_x/TiO_2(800–400)–Pt(0.5)	16	A/R	2.4
5	RhO_x/TiO_2(900–400)–Pt(0.5)	5.6	R	0.56
6	RhO_x/TiO_2(500–400)–Pt(0.2)	89	A	3.8
7	RhO_x/TiO_2(500–400)–Pt(0.3)	89	A	5.0
8	RhO_x/TiO_2(500–400)–Pt(0.4)	89	A	6.1
9	RhO_x/TiO_2(500–400)–Pt(0.6)	89	A	6.0
10	RhO_x/TiO_2(500–400)–Pt(0.8)	89	A	5.0

[a] A: anatase, R: rutile.

 This journal is © The Royal Society of Chemistry 2025

Open Access Article. Published on 22 October 2025. Downloaded on 4/23/2026 1:04:59 PM.
This article is licensed under a Creative Commons Attribution-NonCommercial 3.0 Unported Licence.

Table 2 Amounts of H_2 produced from various alcohol suspensions of RhO_x/TiO_2(500–400)–Pt(0.5) under irradiation of light from Xe lamp with cut filter Y-43 for 3 h

Entry	Alcohols	H_2/μmol
1	Methanol	3.6
2	Ethanol	2.3
3	1-Propanol	3.6
4	1-Butanol	3.0
5	1-Octanol	0.33
6	2-Propanol	8.4
7	2-Butanol	6.5
8	2-Pentanol	4.8
9	Cyclohexanol	2.2
10	Benzyl alcohol	0.54
11	1-Phenylethanol	0.39
12	2-Phenylethanol	0.28

1-propanol, 1-butanol, and 1-octanol), secondary aliphatic alcohols (2-propanol, 2-butanol, and 2-pentanol), alicyclic alcohol (cyclohexanol), primary aromatic alcohols (benzyl alcohol and 2-phenylethanol), secondary aromatic alcohol (1-phenylethanol). These results demonstrate that the RhO_x/TiO_2–Pt photocatalyst has a broad substrate scope for visible-light-driven alcohol dehydrogenation. For example, in the case of benzyl alcohol (entry 10), 0.54 μmol of H_2 was generated after 3 h of irradiation. After 20 h, 3.5 μmol of H_2 was detected in the gas phase, while 3.6 μmol of benzaldehyde was found in the liquid phase. The close agreement between the amounts of H_2 and benzaldehyde confirms the stoichiometric dehydrogenation of benzyl alcohol, as described by eqn (3):

$$C_6H_5CH_2OH \rightarrow C_6H_5CHO + H_2. \quad (3)$$

This result also indicates that benzaldehyde remained stable under the reaction conditions and was not further oxidized to benzoic acid, despite its known susceptibility to oxidation. The sustained high selectivity toward benzaldehyde highlights the mild and controlled nature of this photocatalytic process.

3.8 Expected reaction mechanism

Electron transfer from Rh species to the TiO_2 substrate under visible light irradiation has been confirmed by electrochemical measurements.[8] Based on these findings, the proposed mechanism for alcohol dehydrogenation, namely, the production of H_2 and the oxidation of alcohols, over the RhO_x/TiO_2–Pt photocatalyst under visible light is illustrated in Fig. 7.

The overall reaction proceeds through the following four steps:

1. Photon absorption: incident visible light is absorbed by the Rh species on the TiO_2 surface.

2. Electron injection: the excited Rh species inject electrons into the conduction band of TiO_2.

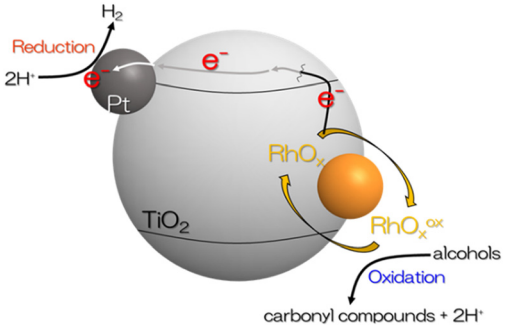

Fig. 7 Expected reaction mechanism for formation of H_2 and carbonyl compounds from various alcohols over RhO_x/TiO_2–Pt photocatalyst under irradiation of visible light.

3. Alcohol oxidation: the resulting electron-deficient Rh species oxidize alcohols to their corresponding carbonyl compounds and are thereby regenerated.

4. H_2 evolution: the injected electrons in the TiO_2 conduction band migrate to the Pt co-catalyst, where protons (H^+) are reduced to generate molecular hydrogen (H_2).

This mechanism highlights the synergistic role of Rh and Pt species: Rh serves as a visible-light sensitizer and oxidation site, while Pt acts as a reduction site for hydrogen evolution.

Conclusions

TiO_2 was successfully modified through the equilibrium adsorption of Rh ions followed by post-calcination, resulting in the formation of RhO_x/TiO_2. The resulting photocatalyst was employed for alcohol dehydrogenation, leading to the production of H_2 and carbonyl compounds under visible light irradiation from an Xe lamp equipped with a Y-43 cutoff filter. The dehydrogenation rate increased significantly upon further modification of RhO_x/TiO_2 with Pt using a colloid impregnation method. In the RhO_x/TiO_2–Pt photocatalyst system, TiO_2 serves as the support, RhO_x acts as the visible-light sensitizer, and Pt functions as the co-catalyst for H_2 evolution. The overall reaction performance was found to depend on three key factors: the pre-calcination temperature, the post-calcination temperature, and the Pt loading. Optimal conditions were identified for each parameter. Among the tested compositions, RhO_x/TiO_2(500–400)–Pt(0.5), based on anatase-phase TiO_2, exhibited the highest H_2 yield. Furthermore, the RhO_x/TiO_2–Pt photocatalyst demonstrated effective activity for the dehydrogenation of a range of alcohols under visible light irradiation.

Author contributions

Atsuhiro Tanaka: conceptualization, formal analysis, writing – original draft, review & editing, supervision, funding acquisition, project administration, final approval of the article. Masaaki Fukuda: investigation, acquisition of data, analysis of data, final approval of the article. Takumi Nagai:

Open Access Article. Published on 22 October 2025. Downloaded on 4/23/2026 1:04:59 PM. This article is licensed under a Creative Commons Attribution-NonCommercial 3.0 Unported Licence.

investigation, acquisition of data, analysis of data, final approval of the article. Hiroyuki Asakura: acquisition of data, analysis and interpretation of data, final approval of the article. Hiroshi Kominami: writing – review & editing, supervision, funding acquisition, project administration, final approval of the article.

Conflicts of interest

There are no conflicts to declare.

Data availability

The data supporting this article have been included as part of the supplementary information (SI). Supplementary information: Fig. S1–S3 See DOI: https://doi.org/10.1039/d5cy00963d.

Acknowledgements

This work was supported by KAKENHI 22H00274, 23H01767 and 23K17964 from the Japan Society for the Promotion of Science. A. T. is grateful for financial support from Proterial Materials Science Foundation. H. K. expresses gratitude for the financial support from Nippon Sheet Glass Foundation for Materials Science and Engineering. XAS experiments were performed at BL01B1, SPring-8 with the approval of JASRI (Proposal No. 2023A1533).

References

1 R. Medhi, M. D. Marquez and T. R. Lee, *ACS Appl. Nano Mater.*, 2020, **3**, 6156–6185.
2 H. Kisch, L. Zang, C. Lange, W. F. Maier, C. Antonius and D. Meissner, *Angew. Chem., Int. Ed.*, 1998, **37**, 3034–3036; H. Kominami, K. Sumida, K. Yamamoto, N. Kondo, K. Hashimoto and Y. Kera, *Res. Chem. Intermed.*, 2008, **34**, 587–601; K. Hashimoto, K. Sumida, S. Kitano, K. Yamamoto, N. Kondo, Y. Kera and H. Kominami, *Catal. Today*, 2009, **144**, 37–41.
3 K. Maeda, K. Ishimaki, Y. Tokunaga, D. Lu and M. Eguchi, *Angew. Chem., Int. Ed.*, 2016, **55**, 8309–8313.
4 N. Murakami, T. Chiyoya, T. Tsubota and T. Ohno, *Appl. Catal., A*, 2008, **348**, 148–152; H. Irie, S. Miura, K. Kamiya and K. Hashimoto, *Chem. Phys. Lett.*, 2008, **457**, 202–205; H. Irie, T. Shibanuma, K. Kamiya, S. Miura, T. Yokoyama and K. Hashimoto, *Appl. Catal., B*, 2010, **96**, 142–147; F. Kuttassery, D. Yamamoto, S. Mathew, S. Remello, A. Thomas, Y. Nabetani, A. Iwase, A. Kudo, H. Tachibana and H. Inoue, *J. Photochem. Photobiol., A*, 2018, **358**, 386–394.
5 H. Yu, H. Irie, Y. Shimodaira, Y. Hosogi, Y. Kuroda, M. Miyauchi and K. Hashimoto, *J. Phys. Chem. C*, 2010, **114**, 16481–16487; Q. Jin, T. Ikeda, M. Fujishima and H. Tada, *Chem. Commun.*, 2011, **47**, 8814–8816; H. Tada, Q. Jin, H. Nishijima, H. Yamamoto, M. Fujishima, S. Okuoka, T. Hattori, Y. Sumida and H. Kobayashi, *Angew. Chem., Int. Ed.*, 2011, **50**, 3501–3505; K. Maeda, K. Ishimaki, M. Okazaki, T. Kanazawa, D. Lu, S. Nozawa, H. Kato and M. Kakihana, *ACS Appl. Mater. Interfaces*, 2017, **9**, 6114–6122; M. Okazaki, Y. Wang, T. Yokoi and K. Maeda, *J. Phys. Chem. C*, 2019, **123**, 10429–10434.
6 E. Reisner, D. Powell, C. Cavazza, J. Fontecilla-Camps and F. Armstrong, *J. Am. Chem. Soc.*, 2009, **131**, 18457–18466; K. Dalle, J. Warnan, J. Leung, B. Reuillard, I. Karmel and E. Reisner, *Chem. Rev.*, 2019, **119**, 2752–2875; H. Moon and K. Yong, *Appl. Surf. Sci.*, 2020, **530**, 147215; A. Charisiadis, V. Nikolaou, E. Nikoloudakis, K. Ladomenou, G. Charalambidis and A. Coutsolelos, *Chem. Commun.*, 2025, **61**, 4630–4646.
7 N. Wang, L. Zhu, Y. Huang, Y. She, Y. Yu and H. Tang, *J. Catal.*, 2009, **266**, 199–206; G. Zhang, G. Kim and W. Choi, *Energy Environ. Sci.*, 2014, **7**, 954–966; D. Won, J. Lee, J. Ji, W. Jung, H. Son, C. Pac and S. Kang, *J. Am. Chem. Soc.*, 2015, **137**, 13679–13690; D. Franchi and Z. Amara, *ACS Sustainable Chem. Eng.*, 2020, **8**, 15405–15429; N. O. Balayeva, Z. Mamiyev, R. Dillert, N. Zheng and D. W. Bahnemann, *ACS Catal.*, 2020, **10**, 5542–5553.
8 S. Kitano, N. Murakami, T. Ohno, Y. Mitani, Y. Nosaka, H. Asakura, K. Teramura, T. Tanaka, H. Tada, K. Hashimoto and H. Kominami, *J. Phys. Chem. C*, 2013, **117**, 11008–11016.
9 S. Kitano, A. Tanaka, K. Hashimoto and H. Kominami, *Phys. Chem. Chem. Phys.*, 2014, **16**, 12554–12559; S. Kitano, A. Tanaka, K. Hashimoto and H. Kominami, *Appl. Catal., A*, 2016, **521**, 202–207.
10 S. Kitano, M. Sadakiyo, K. Kato, M. Yamauchi, H. Asakura, T. Tanaka, K. Hashimoto and H. Kominami, *Appl. Catal., B*, 2017, **205**, 340–346.
11 H. Kominami, A. Furusho, S. Murakami, H. Inoue, Y. Kera and B. Ohtani, *Catal. Lett.*, 2001, **76**, 31–34.
12 H. Kominami, S. Yamamoto, K. Imamura, A. Tanaka and K. Hashimoto, *Chem. Commun.*, 2014, **50**, 4558–4560.
13 R. Singh and S. Dutta, *Fuel*, 2018, **220**, 607–620; F. Bhom and Y. Isa, *Glob. Chall.*, 2024, **8**, 2400134.
14 T. Hisatomi and K. Domen, *Nat. Catal.*, 2019, **2**, 387–399.
15 K. Imamura, H. Tsukahara, K. Hamamichi, N. Seto, K. Hashimoto and H. Kominami, *Appl. Catal., A*, 2013, **450**, 28–33; Z. Liu, J. Caner, A. Kudo, H. Naka and S. Saito, *Chem. – Eur. J.*, 2013, **19**, 9452–9456; M.-Y. Qi, M. Conte, M. Anpo, Z.-R. Tang and Y.-J. Xu, *Chem. Rev.*, 2021, **121**, 13051–13085.
16 H. Kominami, M. Kohno, Y. Takada, M. Inoue, T. Inui and Y. Kera, *Ind. Eng. Chem. Res.*, 1999, **38**, 3925–3931.
17 G. Frens, *Nat. Phys. Sci.*, 1973, **241**, 20–22.
18 A. Tanaka, A. Ogino, M. Iwaki, K. Hashimoto, A. Ohnuma, F. Amano, B. Ohtani and H. Kominami, *Langmuir*, 2012, **28**, 13105–13111.
19 B. Ravel and M. Newville, *J. Synchrotron Radiat.*, 2005, **12**, 537–541.

 This journal is © The Royal Society of Chemistry 2025